Catalysis Today 149 (2010) 372–379

Contents lists available at ScienceDirect

Catalysis Today

journal homepage: www.elsevier.com/locate/cattod

A comparative study of the water gas shift reaction over platinum catalysts supported on CeO_2, TiO_2 and Ce-modified TiO_2

I.D. González [a,*], R.M. Navarro [a,*], W. Wen [b], N. Marinkovic [c], J.A. Rodriguéz [b], F. Rosa [d], J.L.G. Fierro [a]

[a] Instituto de Catálisis y Petroleoquímica (CSIC), Cantoblanco, 28049 Madrid, Spain
[b] Chemistry Department, Brookhaven National Laboratory, Upton, NY 11973, USA
[c] Department of Chemical Engineering, University of Delaware, Newark, DE 19716, USA
[d] Centro experimentación de "El Arenosillo" (CEDEA), INTA Huelva, Spain

ARTICLE INFO

Article history:
Available online 2 September 2009

Keywords:
WGS
Pt
Cerium oxide
Titanium oxide

ABSTRACT

WGS reaction has been investigated on catalysts based on platinum supported over CeO_2, TiO_2 and Ce-modified TiO_2. XPS and XANES analyses performed on calcined catalysts revealed a close contact between Pt precursors and cerium species on CeO_2 and Ce-modified TiO_2 supports. TPR results corroborate the intimate contact between Pt and cerium entities in the Pt/Ce–TiO_2 catalyst that facilitates the reducibility of the support at low temperatures while the Ce–O–Ti surface interactions established in the Ce-modified TiO_2 support decreases the reduction of TiO_2 at high temperature. The changes in the support reducibility leads to significant differences in the WGS activity of the studied catalysts. Pt supported on Ce-modified TiO_2 support exhibits better activity than those corresponding to individual CeO_2 and TiO_2-supported catalysts. Additionally, the Ce–TiO_2-supported catalyst displays better stability at reaction temperatures higher than 573 K that observed on pure TiO_2-supported counterpart. Activity measurements, when coupled with the physicochemical characterization of catalysts suggest that the modifications in the surface reducibility of the support play an essential role in the enhancement of activity and stability observed when Pt is supported on the Ce-modified TiO_2 substrate.

1. Introduction

The water gas shift reaction (WGS, Eq. (1)) and the corresponding low- and high-temperature catalysts, $Cu/ZnO/Al_2O_3$ and Fe_2O_3–Cr_2O_3, respectively, are well established in the hydrogen production schemes at industrial scale.

$$CO + H_2O \leftrightarrow CO_2 + H_2O, \quad \Delta H = -41.1\ \text{kJ/mol} \tag{1}$$

The renewed interest in the WGS reaction has grown significantly during the last few years as a result of the recent advances in fuel cell technology and the need for developing small-scale fuel processors capable of converting *"in situ"* carbonaceous fuels into hydrogen. The role of the WGS reactor in the fuel processors is to provide a primary CO cleanup step and also acts as a secondary reaction to produce hydrogen. Conventional WGS catalysts cannot be applied to small-scale fuel processors because of its complex activation protocol and its instability under air. This new application of the WGS reaction to fuel processing has led to extensive research with the objective to improve catalyst activity and stability over a wider operating temperature than is currently possible with the commercial low-temperature catalysts. In general, it is agreed that both the metal and the support play essential roles in the WGS reaction. Consequently, a number of recent studies have focused on new WGS catalysts based on precious metal catalysts, including Pt, Rh, Pd and Au supported on oxide and mixed oxide supports [1–6]. Supported platinum catalysts have received much interest during last decades because their WGS activity at low temperatures. For Pt-based WGS catalysts, the oxide support is essential to adsorb and activate water due to the thermodynamic instability of PtO_x species under WGS conditions [7]. Therefore, the WGS activity has been measured over Pt-based catalysts deposited on various substrates such as CeO_2 [8–11], ZrO_2 [12,13], CeO_2–ZrO_2 [14,15] and TiO_2 [16–21]. Among the supports examined in bibliography, the CeO_2 and TiO_2 substrates are two of the most promising candidates for water gas shift reaction. Pt/CeO_2 is a promising WGS catalyst but this catalyst deactivates with time on stream. Loss of active metal surface [23], irreversible "over"-reduction of ceria by H_2 [24] or formation of carbonate and/or formate on ceria surface [12] have been proposed as cause of the deactivation of Pt/CeO_2 catalysts. Pt/TiO_2 catalysts are even more active than Pt/CeO_2 counterpart but like the latter these catalysts also deactivated under WGS

* Corresponding authors.
E-mail address: r.navarro@icp.csic.es (R.M. Navarro).

0920-5861/$ – see front matter © 2009 Elsevier B.V. All rights reserved.
doi:10.1016/j.cattod.2009.07.100

conditions. Detailed studies performed on Pt/TiO_2 catalysts applied to WGS have shown that the loss of Pt surface area under reaction conditions is the cause of the catalysts deactivation [19,25]. In order to overcome the stability problems associated to Pt/CeO_2 and Pt/TiO_2 catalysts is essential to stabilize under WGS conditions the Pt metal dispersion and the ability of the support to reversibly exchange oxygen. The surface properties of TiO_2 support are primarily dependent upon various factors such as particle size, structural defects/distortion and the presence of other metal oxide in the surface. It is well known that the surface properties of a metal oxide may be modified with the incorporation of another metal oxide to form mixed oxides at surface level. In this sense there are several reports studying the surface modification of TiO_2 with cerium ions. Cerium ions are particularly interesting to mix with TiO_2 due to the catalytic properties associated to the redox pair Ce^{3+}/Ce^{4+} and because the Ti^{4+} ions can be replaced for cerium ions improving the thermal resistance to sintering and redox properties of TiO_2 [22,26,27].

With this background, in this work the structure and activity of platinum catalyst supported on cerium-modified TiO_2 is compared to that supported on pure CeO_2 and TiO_2 in order to elucidate the role of this type of support into the water gas shift mechanism. The effect of support on the textural, structural and surface catalyst properties were determined by N_2 adsorption–desorption isotherms, XRD, TPR, EXAFS and XPS techniques and related to the activity results in the WGS reaction of gas mixtures simulating typical compositions of reformate streams.

2. Experimental

2.1. Catalyst preparation

TiO_2 support (titanium (IV) oxide, catalyst support Alfa Aesar) was stabilized by thermal treatment at 773 K for 4 h. High surface area CeO_2 support was prepared by the urea coprecipitation-gelation method [28]. Following precipitation, the solid was dried at 383 K for 4 h and, finally calcined in air at 923 K for 8 h. The Ce-modified TiO_2 support ($Ce–TiO_2$, Ce/Ti atomic ratio = 0.032) was prepared by wet impregnation of thermal stabilized TiO_2 powders with aqueous solution of cerium nitrate (Alfa Aesar, Reacton 99.5%). The ceria loading used in the $Ce–TiO_2$ support was selected from preliminary studies performed in our laboratory varying the Ce/Ti atomic ratio between 0.005 and 0.07 (the reported Ce/Ti atomic ratio for monolayer covering on TiO_2 [29]). After cerium impregnation the solid was calcined under air at 873 K for 8 h. Supported Pt catalysts (0.5 wt% metal) were prepared by impregnating each of the above supports under stirring at 353 K for 2 h using aqueous solutions of H_2PtCl_6 metal precursor (Aldrich, 99.9%). After Pt-loading, the samples were calcined in air at 773 K for 3 h. The samples were designated Pt/TiO_2, Pt/CeO_2, $Pt/Ce–TiO_2$ for platinum supported on TiO_2, CeO_2 and Ce-modified TiO_2, respectively.

2.2. Catalyst characterization

The chemical composition of the catalysts was determined by inductively coupled plasma atomic emission spectroscopy (ICP-AES), using a Perkin-Elmer Optima 3300DV apparatus. The samples were first dissolved in acid solutions (a mixture of HF, HCl and HNO_3), microwaved for 15 min, and diluted to concentrations within the detection range of the instrument.

The specific surface areas of the catalysts were calculated by applying the BET method to the N_2 adsorption isotherms measured at liquid nitrogen temperature on a Micromeritics ASAP 2100 apparatus on samples previously degassed at 473 K for 24 h. BET specific areas were calculated from these isotherms using the BET method and taking a value of 0.162 nm^2 for the cross-section of the physically adsorbed N_2 molecule.

X-ray diffraction patterns were recorded using a Seifert 3000P vertical diffractometer and nickel-filtered CuKα radiation (λ = 0.1538 nm) under constant instrument parameters. For each sample, Bragg angles between 5° and 80° were scanned. A rate of 5 s per step (step size: 0.04° 2θ) was used during a continuous scan in the abovementioned range. Volume-averaged crystallite sizes were determined by applying the Debye–Scherrer equation.

Temperature programmed reduction experiments were obtained by heating the samples under a H_2/Ar flow in a U-shaped quartz reactor connected to a Balzer Prisma quadrupole mass spectrometer (QMS200) for on-line gas analysis. Prior to TPR experiments, the samples (about 30 mg) were treated thermally under an air flow at 573 K to remove water and other contaminants. TPR profiles were obtained by heating the samples under a 10% H_2/Ar flow (50 mL/min) from 233 to 1173 K at a linearly programmed rate of 10 K/min.

Platinum dispersion was measured by H_2 chemisorption at 193 K, to minimize contribution of hydrogen spillover, using a dynamic method as described elsewhere [30]. Prior to chemisorption, all samples were reduced under H_2/Ar flow (50 mL/min) for 1 h at 523 K and subsequently flushed under Ar for 15 min at 15 K above the reduction temperature. To calculate metal dispersion, chemisorption stoichiometry of H/Pt = 1 was assumed [31].

X-ray photoelectron spectroscopy (XPS) was used to study the chemical composition and oxidation state of the catalyst surfaces. Photoelectron spectra were recorded with a VG Escalab 200R electron spectrometer equipped with a MgKα X-ray source ($h\nu$ = 1253.6 eV) and a hemispherical electron analyser operating at constant transmission energy (50 eV). The X-ray source was operated at low X-ray fluxes in order to minimize X-ray-induced reduction of Pt and Ce species. The energy regions of Ti 2p, Ce 3d and Pt 4f core-levels in oxidised and reduced samples were recorded. The C 1s peak at 284.6 eV was used as an internal standard for peak position measurement. The areas of the peaks were estimated by calculating the integral of each peak after subtracting a Shirley background and fitting the experimental peak to a combination of Lorentzian/Gaussian lines of variable proportions.

Pt L_{III}-edge, Ce L_{III}-edge and Ti K-edge XAFS spectra were recorded in air at room temperature and *in situ* under different operation conditions, at X-18B and X-19A at the National Synchrotron Light Source (NSLS) at Brookhaven National Laboratory (BNL Upton, New York) [32,33]. The samples, in the amount of 15–25 mg, were loaded into a flow cell (Kapton tube) [34], which was leaked to a 0–100 amu RGA quadrupole Mass Spectrometer (QMS, Stanford Research Systems) for product analysis, and was heated by a heat-blower. The X-ray absorption spectra were taken repeatedly in the "fluorescence yield mode" using a pips detector cooled with circulating water. XAFS data have been analyzed using the Athena program [35]. The *in situ* XANES (X-ray absorption near edge spectroscopy) spectra were recorded during reduction at 473 K with CO and under water gas shift conditions (CO 5%, H_2O 14%, He balance) at 523 K. EXAFS (extended X-ray absorption fine structure) spectra of Pt L_{III}-edge obtained on the fresh calcined catalysts were recorded at room temperature.

2.3. Catalytic activity measurements

The catalysts were tested for the water-gas shift reaction of gas mixtures simulating typical compositions of reformate streams (H_2 28%, CH_4 0.1%, CO 4.4%, CO_2 8.7% N_2 29.2%, H_2O 29.6 vol.%) under a gas hourly space velocity of 21,200 L h^{-1} kg_{cat}^{-1}. Activity tests were performed using 0.2 g of catalyst diluted with SiC (both in the 0.2–0.3 mm particle size range and selected after preliminary mass

transport experiments to minimize diffusional resistances) at a volume ratio of 2:1 to avoid adverse thermal effects. The catalyst bed was placed in a 4 mm ID quartz tubular reactor with a coaxially centered thermocouple. Prior to reaction, the catalysts were flushed in nitrogen at 393 K, followed by reduction *in situ* at 523 K for 2 h (heating rate 5 K/min) with 50 mL(STP)/min of a 10 vol.% H_2/N_2 mixture. The WGS reaction was carried out at atmospheric pressure and temperatures between 498 and 603 K. The efluents of the reactor were analysed by on-line gas-chromatography.

3. Results

3.1. Chemical composition and textural properties

Table 1 shows the chemical compositions, expressed as weight percentages, of calcined catalysts obtained from ICP-AES analyses. For all samples, the chemical compositions were close to the target loading (Pt = 0.5 wt%; CeO_2 in Ce–TiO_2 = 6.5 wt%). The textural properties of the supports (S_{BET} and pore volume), also summarized in Table 1, show that the incorporation of cerium to TiO_2 produces an increase in the surface area and pore volume respect to those corresponding to bare TiO_2. The modification of the textural properties following the addition of cerium to TiO_2 might be due to modifications in the size or porosity of TiO_2 particles or to the segregation of ceria entities on the TiO_2 surface that develop porosity and contribute to the measured specific area.

The specific surface area for the Pt-loaded catalysts show similar values for all supports (Table 1). Comparing the textural properties of the Pt-loaded catalysts with the bare supports indicate that the surface area of CeO_2 and Ce–TiO_2 supports decrease slightly upon incorporating Pt precursors. On the contrary, the TiO_2-supported catalyst suffers a slight recovery in the surface area value respect to the pure TiO_2 support.

3.2. X-ray diffraction

Fig. 1 shows the X-ray diffraction patterns of the calcined supports. The CeO_2 support (C in Fig. 1) exhibits typical diffraction pattern of crystalline cubic cerianite phase (JCPDS 34-394) while the XRD profile of TiO_2 support (T in Fig. 1) shows reflections at 2Θ angles of 25.3°, 37.8° and 48.1° assigned to crystalline anatase phase (JCPDS 84-1286). The Ce-modified TiO_2 support (T–C in Fig. 1) presents reflections of crystalline anatase phase with a very weak peaks around 28.5° and 33.1° corresponding to the strongest line [1 1 1] of the cubic cerianite phase (JCPDS 34-394). The appearance of crystalline ceria structures in the Ce–TiO_2 support indicates the saturation of the capacity of the TiO_2 to accommodate the ceria loading. This is surprising because cerium exists in the form of a two-dimensional overlayer on titania, which cannot be detected by XRD for cerium loadings up to 7.2 Ce^{4+}/nm^2 [29]. From the XRD pattern of Ce–TiO_2 support it is observed that the addition of Ce produces a decrease in the crystalline particle size of TiO_2 (Table 2) without changes in its lattice parameters that dismiss the formation of crystalline $Ti_{1-x}Ce_xO_2$ solid solutions. The appearance of ceria structures together with the decrease in the particle size of TiO_2 are consistent with the above BET result that shows the increase in the surface area after the incorporation of cerium to TiO_2.

The XRD patterns of the platinum-containing samples (not presented here) showed the crystalline phases already detected in the Pt-free supports with no detectable phases due to platinum species.

3.3. Temperature programmed reduction

Reducibility of supports and catalysts were studied by H_2-TPR-MS (Fig. 2). The H_2 consumption profile corresponding to TiO_2 support (Fig. 2A(b)) shows a broad band centered at 919 K with simultaneous H_2O evolution indicative of some surface reduction. MS trace for H_2O also shows a strong peak at 564 K without H_2 consumption which can be assigned to the thermal surface dehydroxylation. The TPR profile for the Ce–TiO_2 support (Fig. 2A(a)) displayed a broad hydrogen consumption peak with components at 879 K and 920 K. Compared with TPR of individual TiO_2, the surface reduction in Ce–TiO_2 support increases in intensity. This hydrogen consumption involves, besides surface reduction of TiO_2 at 920 K, the reduction of cerium ions that, in accordance with the literature addressing reducibility of ceria, may be related with easily reducible surface oxygen from ceria entities of low particle size or with the reduction of some Ce–O–Ti surface structures [22–36].

The reduction profiles of platinum catalysts supported on TiO_2, CeO_2 and Ce–TiO_2 are depicted in Fig. 2B. For the Pt/CeO_2 catalyst, the reduction of Pt starts at 480 K, whereas for the Pt/TiO_2 and the Pt/Ce–TiO_2 samples the reduction is complete at substantially lower temperature (380 K). Calcination treatment of samples after platinum impregnation leads to the formation of platinum oxides (PtO_x) with different stoichiometry depending on the type of

Table 1
Textural properties and chemical composition (wt%) of supports and catalysts and platinum metal dispersion on reduced catalysts.

	BET area (m^2/g)	Pore volume (cm^3/g)	Pt (wt%)	CeO_2 (wt%)	Pt dispersion (%)
CeO_2	65	0.165			
TiO_2	62	0.232			
Ce–TiO_2	70	0.306		6.6	
Pt/CeO_2	62	0.150	0.49		54
Pt/TiO_2	65	0.249	0.52		57
Pt/Ce–TiO_2	65	0.312	0.56	6.7	60

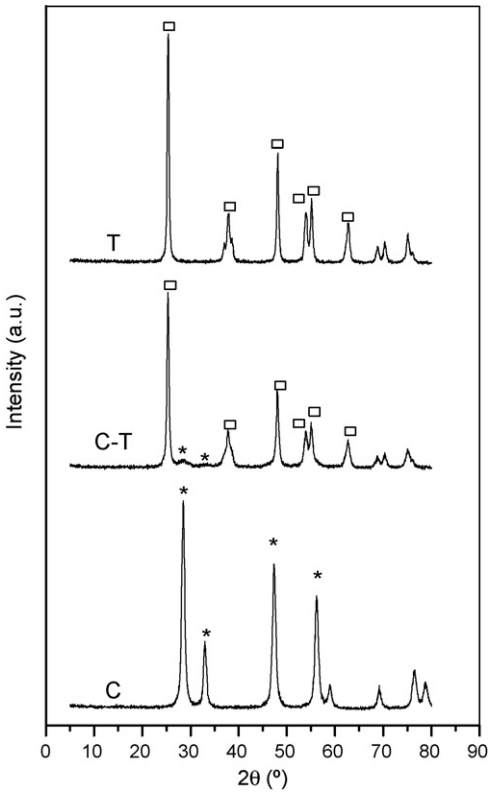

Fig. 1. Powder X-ray diffraction patterns of TiO_2 (T), Ce–TiO_2 (T–C) and CeO_2 (C) supports ((□) anatase, (*) cerianite).

Table 2
CeO_2 and TiO_2 crystalline particle size[a] from XRD patterns of calcined supports and catalysts.

	CeO_2		TiO_2	
	2θ (°)	dp (nm)	2θ (°)	dp (nm)
CeO_2	28.5	13		
TiO_2			25.3	23
Ce–TiO_2	n.d.		25.3	18
Pt/CeO_2	28.5	13		
Pt/TiO_2			25.3	23
Pt/Ce–TiO_2	n.d		25.3	20

[a] The crystalline particle size was estimated using the 2θ lines indicated in the table.

support and oxidation temperature [37–39]. PtO_x species were reduced at temperatures below 523 K with reduction temperature depending on their stoichiometry and interaction with support [37–39]. According to that, the reduction peak at 480 K observed for Pt/CeO_2 catalyst could be assigned to the reduction of surface PtO_x species while the reduction peaks at lower temperature observed for the sample supported on TiO_2 and Ce-modified TiO_2 are attributed to the reduction of PtO_x species with lower stoichiometry (PtO). Quantitative TPR results of Pt/Ce–TiO_2 catalyst indicates that reduction peak at 380 K includes Pt species together with species of support since the measured value of hydrogen consumption ($N_{H_2}/N_{Pt} = 2.4$, where N_{H_2} = number of H_2 molecules consumed and N_{Pt} = number of Pt atoms) was higher than the amount expected for the complete reduction of platinum precursors to Pt^0 ($N_{H_2}/N_{Pt} < 1$). The support species involved in this reduction are related to cerium phases because the intensity of the reduction increases with the ceria content (results from studies performed in our laboratory varying the Ce/Ti ratio not shown here). The reduction of platinum species and the concomitant ceria surface reduction indicate a close interaction between Pt and ceria surface phases. The second hydrogen consumption peak on Pt/Ce–TiO_2 observed at 634 K could be attributed to the reduction of the surface oxygen of TiO_2. This reduction step shift towards higher temperature respect to the reduction temperature observed during the reduction of Pt/TiO_2 catalyst. The modification of Ti reducibility by the presence of Ce is indicative of some Ce–O–Ti surface interaction.

3.4. X-ray photoelectron spectroscopy

XPS analyses performed on calcined TiO_2, CeO_2 and Ce–TiO_2 supports shows a close contact between titanium and cerium atoms in the mixed support. The XPS spectrum of the Ce 3d level for the Ce–TiO_2 support is substantially different from that of the bare CeO_2 counterpart. In the case of the Ce–TiO_2 support, the Ce 3d level shows an increase in the $Ce3d_{5/2}$ binding energy respect to the value observed for bulk CeO_2 (881.5 eV) that may be indicative of a change in the coordination number of the Ce atoms. The Ce 3d spectra of the cerium-containing supports consisted of several peaks resulting from either multiple splitting [40] or shake-up processes [41]. The isolated peak in the Ce 3d spectra at ca. 917 eV (u‴ using the nomenclature of Burroughs [42]) was used as identification of Ce^{4+} species and its relative peak area contribution to total Ce 3d area as a quantitative measure of the amount of Ce^{4+}. The fraction of the total Ce signal attributable to the u‴ peak in the Ce–TiO_2 support sample (4.3% Table 3) is lower than the 14.6% observed for pure CeO_2 support, implying the presence of Ce^{3+} species (ca. 10%) that does not occur in the pure CeO_2 substrate. The stabilization of Ce^{3+} ions on TiO_2 may be consequence of different factors such as small particle size ceria entities [43], a change in coordination of the Ce atoms [44] and/or a net charge due to anion sharing with TiO_2. Considering both the low temperature of calcination used and the difference of ionic radii between Ti^{4+} and Ce^{3+} ions, the stabilization of cerium by its incorporation into the titania lattice appears unlikely. Therefore, the formation of Ti–O–Ce bonds in an interfacial phase $Ce_{1-x}Ti(IV)O_{2-y}$, as reported and explained in earlier literature reports [22,45], is, probably, the type of surface interaction responsible of the reducibility of cerium ions detected by XPS on the Ce–TiO_2 support.

Analysis of the Pt 4f XPS level also indicates modifications in the chemical state and surface distribution of platinum species

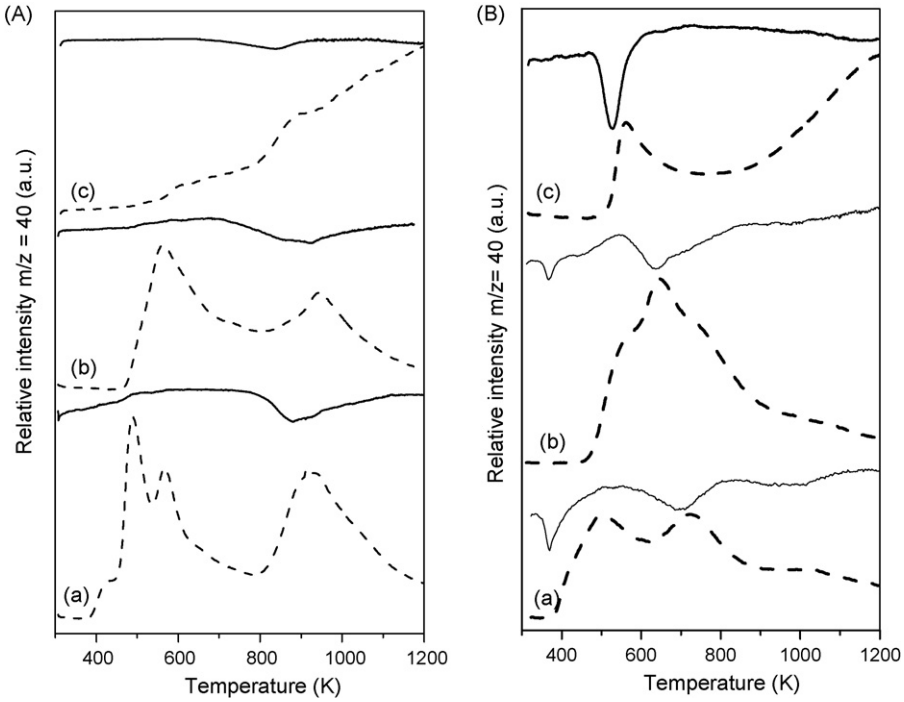

Fig. 2. Signals of H_2 consumption (—) and H_2O production (- - -) obtained during TPR-MS: (A) (a) Ce–TiO_2, (b) TiO_2 and (c) CeO_2; (B): (a) Pt/Ce–TiO_2, (b) Pt/TiO_2 and (c) Pt/CeO_2.

Table 3
Binding energies (eV) of core electrons and surface atomic ratios of calcined and reduced Pt supported catalysts.

	Pt $4f_{7/2}$	Ti $2p_{3/2}$	Ce $3d_{5/2}$ (%u‴ in Ce 3d)	Pt/Ce	Pt/Ti	Ce/Ti
CeO_2						
Calcined			881.5 (14.6)			
TiO_2						
Calcined		458.5				
Ce–TiO_2						
Calcined		458.5	882.1 (4.3)			0.171
Pt/CeO_2						
Calcined	72.4 (53.8%)		881.4 (14.2)	0.012		
	73.1 (46.1%)					
Reduced	70.9 (36.9%)		881.4 (9.7)	0.004		
Pt/TiO_2						
Calcined	72.0 (63.1%)					
	71.7 (28.8%)	458.4			0.007	
	73.0 (71.2%)					
Reduced	71.1 (100%)	458.4			0.002	
Pt/Ce–TiO_2						
Calcined	71.9 (23.2%)	458.7		0.854	0.094	0.110
	73.4 (76.7%)		882.0 (4.8)			
Reduced	71.5 (100%)	458.5		0.126	0.009	0.071

depending on the support used to disperse the metal (Table 3). In calcined samples, the Pt 4f level was resolved into two sets of spin-orbit doublets at 71.7–71.9 eV and 72.4–73.4 eV. The peak at higher binding energy is related to oxidized species of platinum (PtO_x, [46]) whereas the peak at 71.7–71.9 may be attributed to platinum particles with lower oxidation degree in close interaction with the support [17]. The percentages of species associated to the two components of the Pt 4f level indicate that the catalyst supported on CeO_2 possesses the higher proportion of species oxidized of platinum (Table 3). For the sample supported on Ce–TiO_2, it is observed a decrease in the Ce/Ti atomic ratio of the support after Pt incorporation (Table 3); this could correspond to preferential coverage of the cerium species with platinum or to the formation of some specific compound between them.

The chemical changes in the catalyst after reduction in H_2 at 573 K were also investigated by XPS. As shown in Table 3, the Pt $4f_{7/2}$ peaks shifted, after the reduction treatment, to binding energies of 70.9–72.0 eV. According to the data in the literature, the component at higher BE is associated with Pt particles in an electron-deficient state [47], whereas those at lower binding energies indicate the presence of Pt^0 species [47]. As seen in Table 3, the sample supported on CeO_2 has the higher proportion of platinum species maintaining some δ^+ character. This may be the consequence of strong interactions between dispersed platinum species and the CeO_2 support, which has been reported to stabilise surface Pt in an oxidised state [47]. In contrast, the sample supported on Ce–TiO_2 shows the higher proportion of metallic Pt after reduction. As it can be seen in Table 3, after the reduction treatment, the XPS Pt/(Ce,Ti) ratios were lower than those obtained from fresh calcined samples. This points to a transformation in particle size or shape of the platinum precursors during the reduction process. The degree of platinum sintering after reduction depends on the support, being the sample supported on Ce–TiO_2 the case that shows the greatest loss of surface platinum during reduction. Combining the XPS Pt/M (M = Ce,Ti) ratios and the peak percentages corresponding to the Pt^0 state, the surface concentration of metallic platinum on reduced samples varies in the following order: Pt/Ce–TiO_2 > Pt/CeO_2 > Pt/TiO_2. Treatment under hydrogen also produced changes in the Ce state, as indicated by the XPS spectra of the Ce 3d region. Reduction under H_2 at 573 K resulted in Ce species with a u‴ percentage in the total Ce 3d region, that indicates the reduction of Ce^{4+} to Ce^{3+}. As shown in Table 3, a substantial reduction of cerium occurred in both samples, being especially important in the case of the Pt/CeO_2 catalyst. The increase in the degree of reduction of ceria as compared to the support alone indicates, as previously observed by TPR, that platinum facilitates ceria surface reduction. This phenomenon is well documented in the literature and implies a close contact between metallic Pt and ceria surfaces.

3.5. Platinum dispersion

The platinum dispersion values determined by H_2 chemisorption are shown in Table 1. Results of H_2 chemisorption measurements show that platinum is well dispersed for all catalyst samples but, as consequence of the different nature of the support, the platinum dispersion increases following the order: Pt/Ce–TiO_2 > Pt/TiO_2 > Pt/CeO_2. This Pt dispersion order calculated by chemisorption are in line with the surface concentration of Pt calculated previously from XPS analyses over reduced catalysts (Table 3).

3.6. EXAFS

Fig. 3 shows the k2-weighted Fourier transform of the Pt L_{III} EXAFS $\chi(k)$ function for calcined catalysts. Pt/CeO_2 and Pt/Ce–TiO_2 catalysts showed peaks at similar positions (Pt–O distance = 1.05 Å) pointing to the presence of the same type of platinum oxide species on these catalysts, which are different to those present in Pt/TiO_2 catalyst that show larger Pt–O distance (2.0 Å). This result suggests that the platinum species in the calcined Pt/Ce–TiO_2 catalyst are preferentially deposited over cerium entities.

Fig. 4 shows Pt L_{III} edge XANES spectra collected *in situ* for the fresh reduced catalysts and under water gas shift reaction conditions at 523 K. The spectrum of the catalyst supported on TiO_2 (Fig. 4A) shows little changes on the platinum state during water gas shift reaction respect to the fresh reduced sample. On the contrary, significant changes on the platinum state are noted for Pt/CeO_2 and Pt/Ce–TiO_2 catalysts (Fig. 4B and C) under reaction conditions respect to the metallic platinum existing on fresh reduced catalysts. A broad decrease in the whiteline intensity is seen during WGS reaction at 523 K compared with the metallic platinum, which is accompanied with a significant shift of the edge

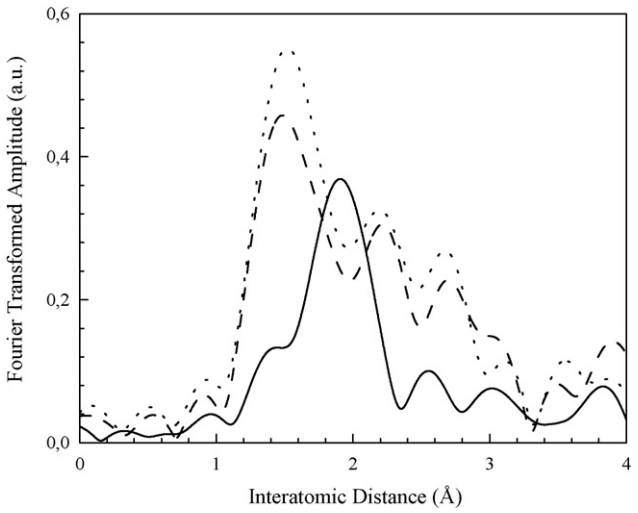

Fig. 3. Pt L_{III} edge EXAFS spectra of calcined catalysts: (–) Pt/TiO_2, (—) $Pt/Ce–TiO_2$ and (. . .) Pt/CeO_2.

jump to higher energies. This result is likely due to enrichment of the electron density of the platinum (caused by an electronic transfer from the support to the platinum centres) or may be associated with changes in the reaction mechanism when ceria is present in the catalyst formulation.

The state of the cerium entities was also studied analyzing the changes on the Ce L_{III} edge XANES spectra of the Pt/CeO_2 (Fig. 5B) and $Pt/Ce–TiO_2$ (Fig. 5A) catalysts during reduction and reaction processes. The fresh calcined catalysts show twin peaks, which is consistent with CeO_2 species. In the spectrum of reduced $Pt/Ce–TiO_2$ catalyst (Fig. 5A) it is observed an increase in the peak intensity around 5728 eV that indicates a substantial reduction of Ce^{4+} to Ce^{3+}. This fact is in line with the higher reducibility detected for this sample in the previous temperature programmed reduction analyses (Fig. 2B). For this sample, under water gas shift conditions a further increase of the peak intensity is observed (Fig. 5A), pointing to the existence of a large portion of Ce^{3+} in the active catalysts.

3.7. Catalytic activity

The CO conversion achieved in the WGS reaction over the Pt catalysts is showed in Fig. 6. It is observed significant differences in WGS activity for the Pt catalysts depending on the support. The Pt/CeO_2 catalyst was significantly the least active catalyst tested reaching a maximum CO conversion of 82% at 593 K. The conversion curve obtained for the Pt/TiO_2 sample was considerably higher than the latter but showed low thermal stability that implies a decrease in its WGS activity for temperatures higher than 573 K. Pt deposited on Ce-modified TiO_2 support exhibits better activity than those corresponding to individual CeO_2 and TiO_2-supported catalysts. Additionally, the $Ce–TiO_2$-supported catalyst displays better stability at reaction temperatures higher than 573 K that that observed on pure TiO_2-supported counterpart.

Turnover frequencies of CO conversion determined taking into account the results of H_2 chemisorption (Table 1) are depicted in Fig. 7. It is observed, in agreement with other studies [3,48–50] that the specific activity of Pt depends on the nature of the support in which is dispersed ($Pt/Ce–TiO_2 > Pt/CeO_2 > Pt/TiO_2$).

4. Discussion

Activity results of the present study show important differences in the specific activity of Pt (Fig. 7) that implies that properties other than the number of metallic platinum sites affect the activity of the catalysts. From recent reports concerning the WGS mechanism over CeO_2 and TiO_2-supported Pt catalysts [21,25,51] it is generally accepted that the WGS reaction occurs with the participation of both metallic phase and support. Over Pt/CeO_2 catalysts, two WGS reaction mechanisms have been proposed: associative and regenerative red-ox mechanism. Kalamaras et al. [21] affirm that the WGS reaction on Pt/TiO_2 catalyst passes through a redox mechanism where CO adsorbs on Pt an reacts with labile oxygen of the TiO_2 while Azzam et al. [51] found that WGS reaction on Pt/TiO_2 follows both (i) a redox and (ii) an associative formate with redox regeneration routes. Whichever is the mechanism operating on the platinum catalysts studied in the present report, it is clear that the reducibility of the catalyst surface is critical for generating the active germinal OH groups on the support (associative mechanism) and/or for generating reducing

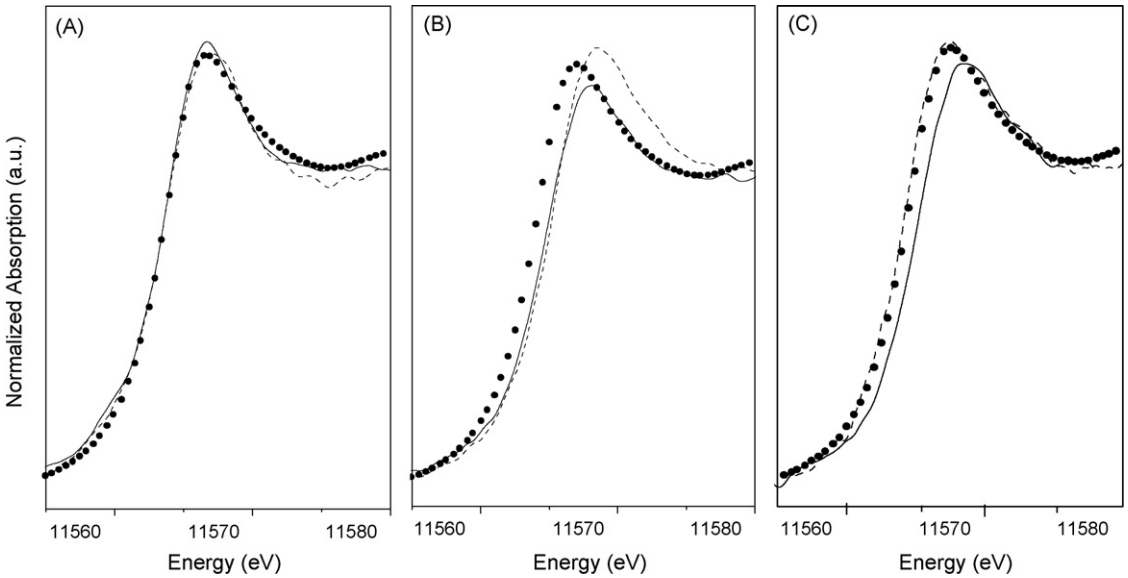

Fig. 4. Pt LIII edge XANES spectra of (A) Pt/TiO_2, (B) $Pt/Ce–TiO_2$ and (C) Pt/CeO_2 catalysts. (●) Pt foil, (- - -), reduced catalysts (under CO at 473 K) and (—) catalysts under WGS conditions at 523 K.

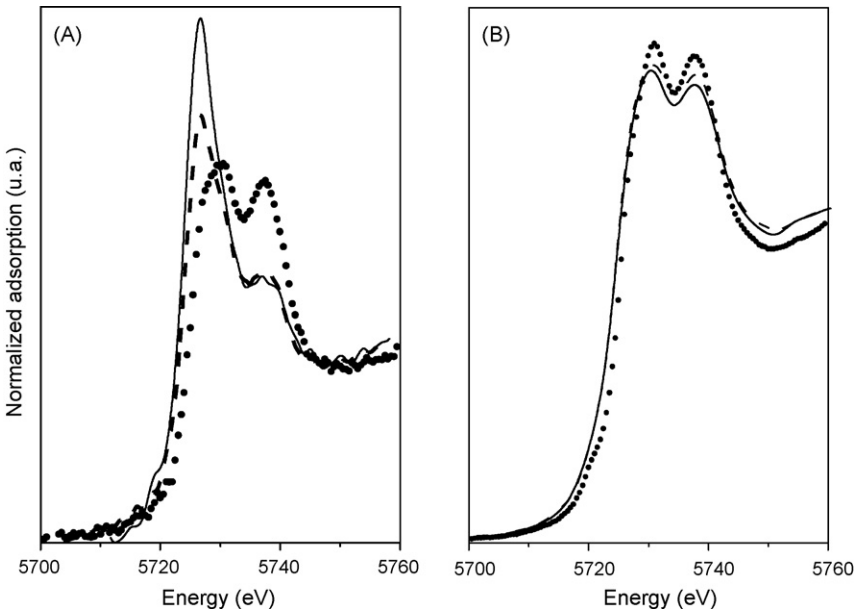

Fig. 5. Ce L_{III} edge XANES spectra of (A) Pt/Ce–TiO_2 and (B) Pt/CeO_2 catalysts. (●) calcined catalysts, (—) reduced catalysts (under CO at 473 K) and (—) catalysts under WGS conditions.

centers which are then reoxidized by water molecules with the simultaneous release of H_2 (redox mechanism).

XRD and XPS data have shown that cerium in the mixed Ce–TiO_2 support is present in a highly dispersed state with a close interaction with Ti atoms. In this situation, platinum oxidized species interacts in a different way to that operating on bare TiO_2. XPS data (Table 3) and Pt L_{III} EXAFS spectra (Fig. 3) of Pt/Ce–TiO_2 catalyst show the preferential interaction of PtO_x species with cerium surface entities. As a consequence of that, better dispersion and uniformity of Pt oxidized species are achieved on this support respect to pure TiO_2 (Tables 1 and 3). The cerium-mediated modification in the interaction of PtO_x species with the support in the Pt/Ce–TiO_2 catalyst also affects the surface reduction of the support respect to those observed on bare TiO_2. As observed in Fig. 2A, the contact between Pt and Ce in the Pt/Ce–TiO_2 catalyst facilitates the reducibility of the support at low temperatures. This better reducibility of the support is also observed under reaction conditions as the analysis of Ce L_{III} edge XANES spectra showed (Fig. 5). The promotion in the reducibility of the support at low temperature observed when platinum is supported on Ce–TiO_2 is in line with the higher activity at low temperature observed for this sample (Fig. 6). The better stability achieved for Pt/Ce–TiO_2 at high reaction temperatures ($T > 548$ K) compared to Pt/TiO_2 could be associated to its different behaviour against the changes that catalysts may suffer under reaction at high temperature. Since Pt-based WGS catalyts are bifunctional, the thermal deactivation of Pt/TiO_2 catalyst can involve Pt and or TiO_2 support. Although TiO_2 is more resistant to reduction than CeO_2, it can be partially reduced under the WGS reaction conditions studied. Several works in literature [52–54] reported that reduction of TiO_2 is possible at temperatures higher than 573 K, resulting in creation of oxygen vacancies (defects) via reduction of the cation charge (Ti^{x+}, $x < 4$) that may decrease the CO chemisorption capacity of platinum affecting its activity. Azzan et al. [19] on the other hand, attributed deactivation of Pt/TiO_2 catalysts to the growth of Pt metal particles during WGS reaction. Taking into account the changes that

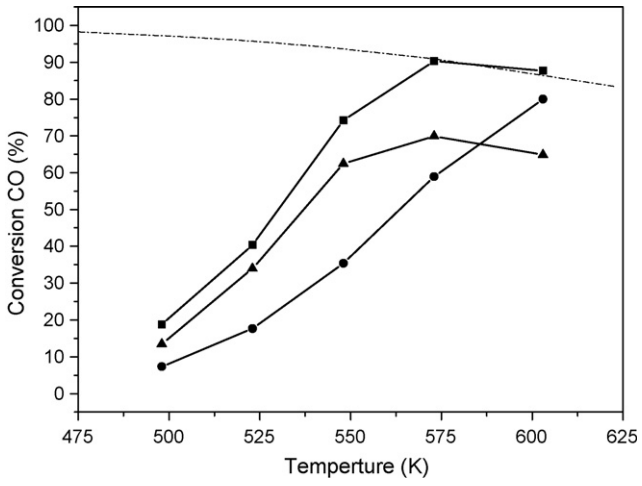

Fig. 6. CO conversion for the WGS reaction on supported Pt catalyst: (●) Pt/CeO_2, (▲) Pt/TiO_2 and (■) Pt/Ce–TiO_2. Reaction conditions: total pressure 1 atm, GHSV = 21,200 L h^{-1} kg cat^{-1}, feed gas composition (% mol): H_2 28%, CH_4 0.1%, CO 4.4%, CO_2 8.7%, N_2 29.2%, H_2O 29.6%. Dotted line shows thermodynamic equilibrium limit.

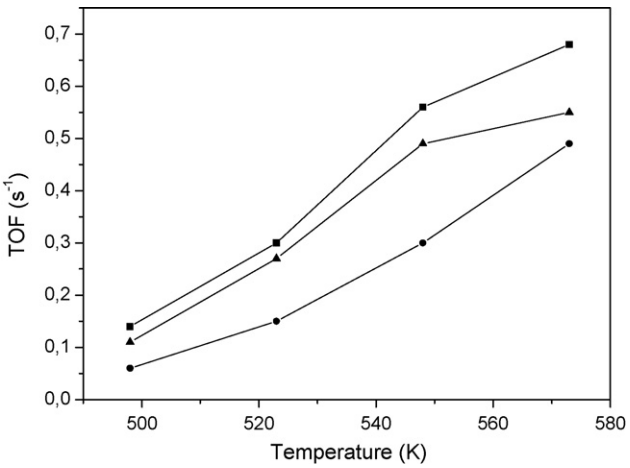

Fig. 7. Turnover frequencies of CO conversion for the WGS reaction on supported Pt catalyst: (●) Pt/CeO_2, (▲) Pt/TiO_2 and (■) Pt/Ce–TiO_2.

catalysts may suffer under reaction at high temperature, the differences in support reducibility and stability of Pt particles associated to the presence of Ce in the Ce-modified support may be the origin of the better thermal stability of the Pt/Ce–TiO_2 catalysts under reaction temperatures higher than 548 K (Fig. 6). TPR data of Pt/Ce–TiO_2 catalyst showed (Fig. 2B) that the presence of cerium decrease the Ti reducibility at high temperature by the development of some Ce–O–Ti surface interaction. The lower reducibility of Ti ions at high temperature in the Ce–TiO_2-supported catalyst may be the origin of the better thermal stability observed for this sample because it may decrease the modification of electronic properties of Pt from its interaction with partially reduced Ti^{3+} sites which is supposed to be the main cause of the deactivation of TiO_2 catalysts at temperatures higher than 548 K.

5. Conclusions

The water gas shift reaction over Pt catalysts supported on TiO_2, CeO_2 and Ce–TiO_2 has been studied. Pt supported on Ce-modified TiO_2 support exhibits better activity than those corresponding to individual ceria and titania supported catalysts. Additionally, the Ce–TiO_2 supported catalyst displays better stability at reaction temperatures higher than 573 K that that observed on pure TiO_2-supported counterpart. Characterization of the catalyst shows that cerium in the Ce–TiO_2 support was present in a highly dispersed state with a close interaction with Ti atoms. The contact between Pt and Ce in the Pt/Ce–TiO_2 catalyst facilitates the reducibility of ceria component in the support at low temperatures and also hinder the overreduction of Ti at high temperature. This modification in the reducibility of the support when platinum is supported on Ce–TiO_2 is proposed to be the cause of the better activity and stability of this sample in the water gas shift reaction.

Acknowledgments

This work is within the framework of the Project "Development of a Diesel fuel Processor" carried out by INTA, AICIA, CIDAUT and the Instituto de Catálisis y Petroleoquímica (CSIC). The research performed at the Chemistry Department of Brookhaven National Laboratory was financed through Contract No. DE-AC02-98CH10086 with the US Department of Energy, Division of Chemical Sciences. The National Synchrotron Light Source (NSLS) is supported by the Divisions on Chemical and Materials Sciences of the US Department of Energy. Dr. Syed Khalid was grateful for his assistance during the EXAFS measurements.

References

[1] J. Barbier, D. Duprez, Appl. Catal. B: Environ. 4 (1994) 105.
[2] R. Dictor, J. Catal. 106 (1987) 458.
[3] D.C. Grenoble, M.M. Estadt, D.F. Ollis, J. Catal. 67 (1981) 90.
[4] S. Hilaire, X. Wang, T. Luo, R.J. Gorte, J. Wagner, Appl. Catal. A: Gen. 215 (2001) 271.
[5] D. Andreeva, I. Ivanova, L. Ilieva, M.V. Abrashev, Appl. Catal. A: Gen. 302 (2006) 127.
[6] S. Golunski, R. Rajaram, N. Hodge, G.J. Hutchings, C.J. Kiely, Catal. Today 72 (2002) 107.
[7] K. Takanabe, K. Aika, K. Seshan, L. Lefferts, J. Catal. 227 (2004) 101.
[8] G. Jacobs, L. Williams, U. Graham, G.A. Thomas, D.E. Sparks, B.H. Davis, Appl. Catal. A: Gen. 252 (2003) 107.
[9] L. Mendelovici, M. Steinberg, J. Catal. 96 (1) (1985) 285.
[10] T. Bunluesin, R.J. Gorte, G.W. Graham, Appl. Catal. B: Environ. 15 (1998) 107.
[11] X.H. Liu, W. Ruettinger, X. Xu, R. Farrauto, Appl. Catal. B: Environ. 56 (2005) 69.
[12] J.M. Pigos, C.J. Brooks, G. Jacobs, B.H. Davis, Appl. Catal. A: Gen. 319 (2007) 47.
[13] D. Tibiletti, F.C. Meunier, A. Goquet, D. Reid, R. Burch, M. Boaro, M. Vicario, A. Trovarelli, J. Catal. 244 (2006) 183.
[14] S. Ricote, G. Jacobs, M. Milling, Y. Ji, P.M. Patterson, B.H. Davis, Appl. Catal. A: Gen. 303 (2006) 183.
[15] W. Ruettinger, X.H. Liu, R.J. Farrauto, Appl. Catal. B: Environ. 65 (2006) 135.
[16] H. Iida, K. Kondo, A. Igarashi, Catal. Commun. 7 (2006) 240.
[17] H. Iida, A. Igarashi, Appl. Catal. A: Gen. 303 (2006) 192.
[18] P. Panagiotopoulou, D.I. Kondarides, J. Catal. 225 (2004) 327.
[19] K.G. Azzam, I.V. Babich, K. Sesham, L. Lefferts, Appl. Catal. A: Gen. 338 (2008) 66.
[20] P. Panagiotopoulou, A. Chistodoulakis, D.I. Kondarides, S. Boghosian, J. Catal. 240 (2006) 114.
[21] C.M. Kalamaras, P. Panagiotopoulou, D.I. Kondarides, A.M. Efstathiou, J. Catal. 264 (2) (2009) 117.
[22] J. Rynkowski, J. Farbotko, R. Touroude, L. Hilaire, Appl. Catal. A: Gen. 203 (2000) 335.
[23] X. Wang, R.J. Gorte, J.P. Wagner, J. Catal. 212 (2002) 225.
[24] J.M. Zalc, V. Sokolovskii, D.G. Löffler, J. Catal. 206 (2002) 169.
[25] Y.T. Kim, E.D. Park, H.C. Lee, D. Lee, K.H. Lee, Appl. Catal. B: Environ. 90 (2009) 45.
[26] G. Dutta, U.V. Waghmare, T. Baidya, M.S. Hegde, K.R. Priolkar, P.R. Sarode, Chem. Mater. 18 (2006) 3249.
[27] T. López, F. Rojas, R. Alexander-Katz, F. Galindo, Z. Balankin, A. Buljan, J. Solid State Chem. 177 (2004) 1873.
[28] L. Kundakovic, M. Flytzani-Stephanopoulos, J. Catal. 179 (1998) 203.
[29] H. Zhu, M. Shen, Y. Kong, J. Hong, Y. Hu, T. Lin, L. Dong, Y. Chen, C. Jian, Z. Liu, J. Mol. Catal. A: Chem. 219 (2004) 155.
[30] M. Ojeda, M. Lopez Granados, S. Rojas, P. Terreros, F.J. Garcia-Garcia, J.L.G. Fierro, Appl. Catal. A: Gen. 261 (2004) 47.
[31] C. Pedrero, T. Waku, E. Iglesia, J. Catal. 233 (2004) 242.
[32] A. Rodriguez, X.Q. Wang, P. Liu, W. Wen, J.C. Hanson, J. Hrbek, M. Perez, J. Evans, Top. Catal. 44 (2007) 73.
[33] X.Q. Wang, J.A. Rodriguez, J.C. Hanson, D. Gamarra, A. Martinez-Arias, M. Fernandez-Garcia, Top. Catal. 49 (2008) 81–88.
[34] P.J. Chupas, M.F. Ciraolo, J.C. Hanson, C.P. Grey, J. Am. Chem. Soc. 123 (2001) 1694.
[35] B. Ravel, M. Newville, J. Synchrotron Rad. 12 (2005) 537.
[36] P.O. Larsson, A. Andersson, J. Catal. 179 (1998) 72.
[37] C.P. Hwang, C.T. Yeh, J. Mol. Catal. A 112 (1996) 295.
[38] T. Huizinga, J. Van Grondelle, R. Prins, Appl. Catal. 10 (1984) 199.
[39] J.Z. Shyu, K. Otto, J. Catal. 115 (1989) 16.
[40] G. Thornton, M.J. Dempsey, Chem. Phys. Lett. 77 (1981) 409.
[41] A. Fujimori, A. Fujimori, J. Magn. Magn. Mater. 47–48 (1985) 24332.
[42] P. Burroughs, A. Hamnett, A.F. Orchard, G. Thornton, J. Chem. Soc., Dalton Trans. 17 (1976) 1686.
[43] A. Laachir, V. Perrichon, A. Badri, J. Lamotte, E. Catherine, J.C. Lavalley, J. Elfallah, L. Hilaire, F. Lenormand, E. Quemere, G.N. Sauvion, O.R. Touret, J. Chem. Soc., Faraday Trans. 87 (1991) 1601.
[44] A. Martinez-Arias, M. Fernandez-Garcia, L.N. Salamanca, R.X. Valenzuela, J.C. Conesa, J. Soria, J. Phys. Chem. B 104 (2000) 4038.
[45] A. Dauscher, P. Wehrer, L. Hilaire, Catal. Lett. 14 (1992) 171.
[46] O.S. Alexeev, S.Y. Chin, M.H. Engelhard, L. Ortiz-Soto, M.D. Amiridis, J. Phys. Chem. B 109 (2005) 23430.
[47] C. Serre, F. Garin, G. Belot, G. Maire, J. Catal. 141 (1993) 1.
[48] K.G. Azzam, I.V. Babich, K. Seshan, L. Lefferts, J. Catal. 251 (2007) 163.
[49] R.J. Gorte, S. Zhao, Catal. Today 104 (2005) 18.
[50] P. Panagiotopoulou, D.I. Kondarides, Catal. Today 112 (2006) 49.
[51] K.G. Azzam, I.V. Babich, K. Seshan, L. Lefferts, J. Catal. 251 (2007) 153.
[52] G.L. Haller, D.E. Resasco, Adv. Catal. 36 (1989) 173.
[53] Y. Li, Y. Fan, H. Yang, B. Xu, L. Feng, M. Yang, Y. Chen, Chem. Phys. Lett. 372 (2003) 160.
[54] M. Calatayud, A. Markovits, M. Menetrey, B. Mguig, C. Minot, Catal. Today 85 (2003) 125.